Minimum Required PV Capacity for Solar-Powered EV Charging: A Case Study of Route Reassignment for Clinic Shuttle Services in Japan

Koki Kumaoka*, Haru Morikawa*,
Nobumasa Matsui**, Jiyoung Choi***, Yuji Mizuno****‡

*Graduate School of Biomedical Engineering, Division of Biomedical Engineering,
Osaka Electro-Communication University, 1130-70 Kiyotaki, Shijonawate, Osaka 575-0063 Japan

**Department of Engineering, Faculty of Engineering,
Nagasaki Institute of Applied Science, 536 Aba-machi, Nagasaki, Nagasaki, 851-0193 Japan

***Department of Applied Information Technology, Faculty of Applied Information Technology,
Nagasaki Institute of Applied Science, 536 Aba-machi, Nagasaki, Nagasaki, 851-0193 Japan

****Department of Health Informatics, Faculty of Health Informatics,
Osaka Electro-Communication University, 1130-70 Kiyotaki, Shijonawate, Osaka 575-0063 Japan

(ML24A005@oecu.jp, ML25A009@oecu.jp, matsui_nobumasa@nias.ac.jp, choi_jiyoung@nias.ac.jp, y-mizuno@osakac.ac.jp)

‡Corresponding Author; Yuji Mizuno, 1130-70 Kiyotaki, Shijonawate, Osaka 575-0063 Japan, Tel: +81 72 876 3317,
y-mizuno@osakac.ac.jp

Received: 15.01.2026 Accepted:12.03.2026

Abstract- This study explores the determination of an appropriate photovoltaic (PV) capacity for charging electric vehicles (EVs) through a case study on the electrification of clinic shuttle services in Japan. The purpose is to evaluate the feasibility of sustaining EV shuttle services using solar energy alone, without dependence on grid electricity, under diverse solar conditions. Recent efforts toward energy efficiency and decarbonization have accelerated the integration of renewable energy technologies and EVs. In the healthcare sector, shuttle services for elderly and mobility-impaired patients are widely operated, and their electrification is increasingly regarded as an important measure for reducing environmental impact. However, EV operation faces challenges related to charging availability and the variability of PV energy generation. This study analyzes the feasibility of photovoltaic-to-vehicle (PV2V) EV shuttle operation under varying meteorological conditions using real-world shuttle operation data. Meteorological conditions are classified into three categories using percentile-based thresholds of daily solar radiation, and month-long charging simulations are conducted using state-of-charge (SoC) trajectories estimated from actual driving records of clinic shuttle services. In addition, the impact of operational strategies is investigated by modifying shuttle route assignments while keeping the number of EVs fixed to reflect actual clinic operations. By redistributing driving distances among vehicles, the effect of operational load balancing on charging feasibility and required PV capacity is evaluated. The results indicate that appropriate route reassignment can significantly reduce the required PV capacity; for example, under low-solar-radiation conditions, the required PV capacity is reduced by approximately 31%.

Keywords photovoltaic; electric vehicles; clinic; photovoltaic to vehicle; solar radiation; state of charge.

1. Introduction

Reducing electricity demand, improving energy efficiency, and accelerating the deployment of renewable energy technologies are widely recognized as fundamental measures for mitigating CO_2 emissions and addressing global climate change [1–4]. In Japan, hospitals represent some of the most energy-intensive facilities, making the reduction of their electricity consumption a critical and urgent issue [5]. Unlike other types of buildings, hospitals are required to operate continuously to ensure uninterrupted medical services, resulting in persistently high energy demand throughout the year. This demand is further amplified by the extensive use of high-power medical devices essential for diagnosis and treatment. Given these characteristics, enhancing energy conservation in hospital facilities is particularly important. In response to this challenge, the Japanese government has actively promoted energy-saving initiatives in the healthcare sector, including the introduction and expansion of renewable energy systems such as photovoltaic (PV) power generation [6–8]. These efforts aim not only to reduce electricity consumption and associated CO_2 emissions, but also to improve the resilience and sustainability of hospital energy systems.

In recent years, the installation of PV systems has expanded rapidly in hospitals and other healthcare-related facilities [9, 10]. Along with this trend, medical institutions have increasingly focused on introducing electric vehicle (EV) shuttle services powered by on-site PV generation as a practical approach to reducing both energy consumption and environmental impact.

A wide range of studies have investigated the integration of renewable energy sources and EVs in power systems. Numerous studies have focused on grid-connected systems that integrate renewable generation, EVs, and stationary energy storage, aiming to reduce electricity costs and grid load while improving economic performance and grid stability through optimized charging and discharging control [11–18]. Other studies have examined EV charging and discharging strategies for demand response and vehicle-to-grid (V2G) applications in power distribution systems, with the objective of enhancing system flexibility and mitigating peak demand [19, 20].

In addition, charging and discharging strategies that balance renewable energy utilization and economic profitability, while explicitly accounting for EV and battery degradation, have been investigated in [21, 22]. Furthermore, demonstration-based studies have evaluated energy flows and economic feasibility of EV charging facilities equipped with PV systems and energy storage at residential, commercial, and urban scales [23–25]. Collectively, these studies demonstrate that the coordinated integration of renewable energy sources, EVs, and energy storage—supported by optimized charging and discharging control—can improve economic performance, reduce grid load and peak demand, enhance system flexibility, and maintain grid stability.

Accordingly, existing research has systematically examined optimal operational strategies for PV–EV integrated systems under grid-connected frameworks, including grid-to-vehicle (G2V) and vehicle-to-grid (V2G) operations. Despite the increasing attention to renewable energy integration in transportation and building energy systems, relatively limited research has investigated the feasibility of PV-based EV charging under strict operational constraints such as those found in healthcare shuttle services. However, the operational energy-management challenges specific to medical facilities providing shuttle services have received little attention. In particular, constraints unique to such applications—such as limited charging time windows imposed by shuttle schedules and fluctuations in PV output due to meteorological factors such as solar radiation and sunshine duration—remain insufficiently investigated.

This study investigates the feasibility of photovoltaic-to-vehicle (PV2V) EV charging operation under varying meteorological conditions. Month-long simulations were performed to evaluate how PV capacity requirements and charging performance depend on solar conditions and operational strategies. To capture realistic operational constraints, the simulations were performed using meteorological categories classified by percentile-based thresholds of daily solar radiation and SoC trajectories estimated from actual shuttle driving records.

A preliminary version of this work was presented in a conference paper [26], which investigated the feasibility of PV2V EV shuttle operation under a winter-solstice scenario using a one-week simulation and focusing primarily on charger configuration. The present study substantially extends that earlier work in several aspects. First, meteorological conditions are systematically classified using a statistical framework based on percentile-based thresholds of daily solar radiation, enabling a more representative evaluation of PV generation variability. Second, the analysis is expanded to month-long simulations using SoC trajectories estimated from actual shuttle driving records, allowing a more comprehensive assessment of operational feasibility under practical driving conditions. Third, the present study introduces an operational load-balancing strategy through shuttle route reassignment and quantitatively evaluates its impact on reducing the required PV capacity. These extensions provide a more comprehensive and practically relevant evaluation of PV2V EV shuttle operation in healthcare facilities.

The simulation comprises four main steps. First, the operational characteristics of the clinic shuttle services are analyzed using actual driving records to define daily driving demand and charging-time constraints. Second, PV energy generation is estimated from solar radiation data by considering panel specifications, temperature effects, and system losses. Third, EV SoC trajectories are computed using a distance-based energy consumption model derived from actual shuttle operation data, allowing the charging feasibility of each vehicle to be evaluated under realistic operating conditions. Finally, the charging process is analyzed under a PV2V operational assumption, and the effects of operational strategies, including shuttle route reassignment, are examined. By redistributing driving distances and return times among vehicles, the analysis evaluates how operational load balancing influences charging feasibility and the required PV capacity.

This study is conducted under several simplifying assumptions to clarify the technical feasibility of PV-based EV charging for clinic shuttle services. First, although grid-connected operation is common in practical systems, electricity supply from the commercial power grid is not considered in this study. Instead, EV charging is assumed to rely solely on PV power generation, corresponding to a PV2V operation, in which electricity generated by the PV system is directly used for EV charging without grid support. This off-grid assumption is adopted to clarify the upper bound of PV capacity requirements and to isolate the impact of charging-time availability on PV-based EV operation. In addition, distributed generators (DGs) and stationary energy storage systems (ESSs) are not included in this study, in order to focus on the impact of PV generation characteristics and charging-time availability on EV operation. Finally, economic aspects such as installation cost and operational cost are not evaluated, as the scope of this study is limited to technical and operational feasibility.

Although the analysis is based on a specific clinic, the proposed evaluation framework—combining statistically classified meteorological conditions with real-world operational data and charging-time constraints—is applicable to other medical and welfare facilities that operate scheduled EV shuttle services. The main contributions of this study are summarized as follows:

1) A statistical evaluation framework for PV capacity requirements is developed by classifying meteorological conditions using percentile-based thresholds of daily solar radiation and examining their relationship with sunshine duration.
2) A realistic month-long EV charging simulation framework is established using actual shuttle operation data and a distance-based energy consumption model to estimate EV SoC trajectories, enabling feasibility assessment under practical operational constraints.
3) The study demonstrates that operational load balancing through shuttle route reassignment can significantly reduce the required PV capacity without increasing the number of EVs or charging equipment, highlighting the importance of operational design in PV2V charging systems.

The remainder of this paper is organized as follows. Section II introduces the target dialysis clinic and describes the operational characteristics of its shuttle services based on actual driving records. Section III presents the PV-based charging control logic and the charging sequence analysis method, including the modeling of PV generation, charging energy allocation, and EV SoC variation. Section IV describes the percentile-based classification of meteorological conditions, the simulation setup, and the charging simulation results under the classified solar radiation conditions. Section V discusses the impact of operational strategies, particularly shuttle route reassignment, on the required PV capacity and further examines the robustness of the results through sensitivity analysis. Finally, Section VI provides the conclusions of this study.

2. Target Clinic

2.1. Clinic Overview

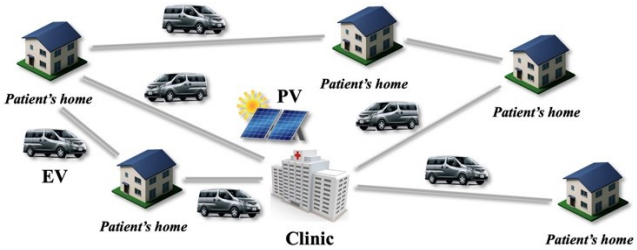

Fig. 1. Schematic diagram of the clinic shuttle services.

Figure 1 shows a schematic diagram of the clinic-operated shuttle services. This study considers the introduction of EVs for the shuttle services provided by the clinic. This clinic specializes in dialysis treatment and provides shuttle services for elderly patients and those with difficulty commuting. The shuttle services connecting the clinic and patients' homes operate six shuttle vehicles Monday through Saturday within a 30 km radius of the clinic. The clinic is closed on Sundays. Based on prior research, the clinic's potential for PV power generation has been estimated by considering rooftop and parking lot installations. These locations are expected to accommodate a total installed capacity of up to 140 kW, providing a feasible foundation for PV2V EV charging [26].

2.2. Monitoring of Shuttles Services Operations

To characterize the operational features of the clinic's shuttle services, actual driving data were collected. Global Positioning System (GPS) loggers were installed on all shuttle vehicles in service, enabling continuous acquisition of positional information and the reconstruction of shuttle service trajectories. Based on these GPS records, the driving routes and travel distances of each vehicle were derived, enabling the estimation of daily travel behavior, trip frequency, and operational range. The GPS data were acquired using i-gotU GPS loggers (GT-600) manufactured by Mobile Action Technology Inc. Figure 2 presents an example of the cumulative driving distances of six shuttle vehicles recorded over a single day. The vertical axis represents the cumulative distance traveled in kilometers, while the horizontal axis denotes time from 6:00 a.m. to 4:00 p.m. Among the six vehicles, Vehicle 4 traveled the longest distance, reaching 90.25 km, whereas Vehicle 6 recorded the shortest distance of 35.49 km.

A notable feature of the operation is the midday interval between the morning and afternoon shuttle services, during which all vehicles remain parked at the clinic. When considering fleet electrification, this idle period becomes particularly important because it provides an opportunity for EV charging. This interval generally corresponds to a period when relatively high PV energy generation can be obtained during the daytime. Consequently, it offers a favorable window for PV2V charging. Effective utilization of this charging opportunity allows multiple EVs to be recharged simultaneously, thereby reducing dependence on grid electricity and supporting the sustainable operation of shuttle services.

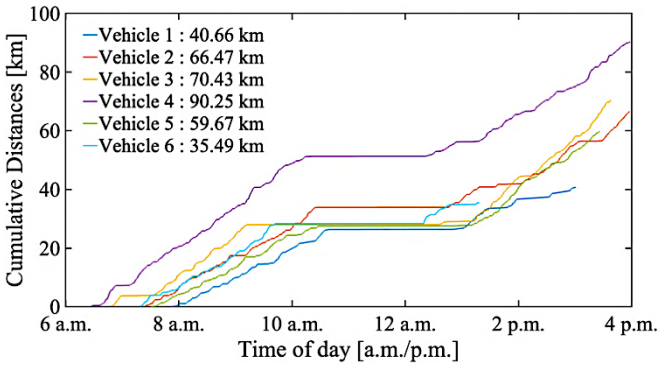

Fig. 2. Example of cumulative distances of six shuttle vehicles over a single day based on actual driving data.

Table 1. Weekly driving distance of each shuttle vehicle

Vehicle ID	*Cumulative Distances [km]*
Vehicle 1	367.95
Vehicle 2	391.63
Vehicle 3	412.43
Vehicle 4	543.13
Vehicle 5	435.29
Vehicle 6	377.31

In addition, Table 1 summarizes the cumulative driving distance of each shuttle vehicle over a one-week period, derived from the GPS-based driving records. As shown in the table, the weekly driving distances differ considerably among the vehicles. Vehicle 4 exhibits the longest cumulative distance (543.13 km), whereas Vehicle 1 records the shortest distance (367.95 km). The maximum difference in weekly driving distance among the Vehicles therefore reaches approximately 175 km, indicating a substantial imbalance in operational load across the fleet. When considering fleet electrification, this variation implies that EVs assigned to longer shuttle routes experience greater energy consumption and tend to return to the clinic later, potentially reducing the available charging time under PV2V operation.

3. Charging Sequence Analysis Method

3.1. Charging Control Logic and Its Flowchart Representation

Figure 3 illustrates the PV2V charging control logic adopted in this study. In the following description, the shuttle vehicles are represented as EVs and are indexed as EV1–EV6 for convenience. On service-operating days, each EV completes its morning shuttle route and returns to the clinic with a reduced SoC. Charging control is activated when the available PV energy in a 5-min time step exceeds the minimum AC charging energy threshold $E_{min,AC}$. This threshold is defined with reference to IEC 61851-1:2017, which specifies the operating requirements for normal conductive AC charging systems, and is adopted in this study as the minimum energy level necessary for stable initiation of AC charging.

Accordingly, two AC chargers are first assigned to EVs in the order of return. After the final EV has returned, the SoC of all vehicles is evaluated, and the EV with the lowest SoC is selected for priority charging using a DC charger within the available PV power range. In this study, DC charging is modeled as power-controllable within the available PV range, and no minimum energy threshold is imposed for DC charging.

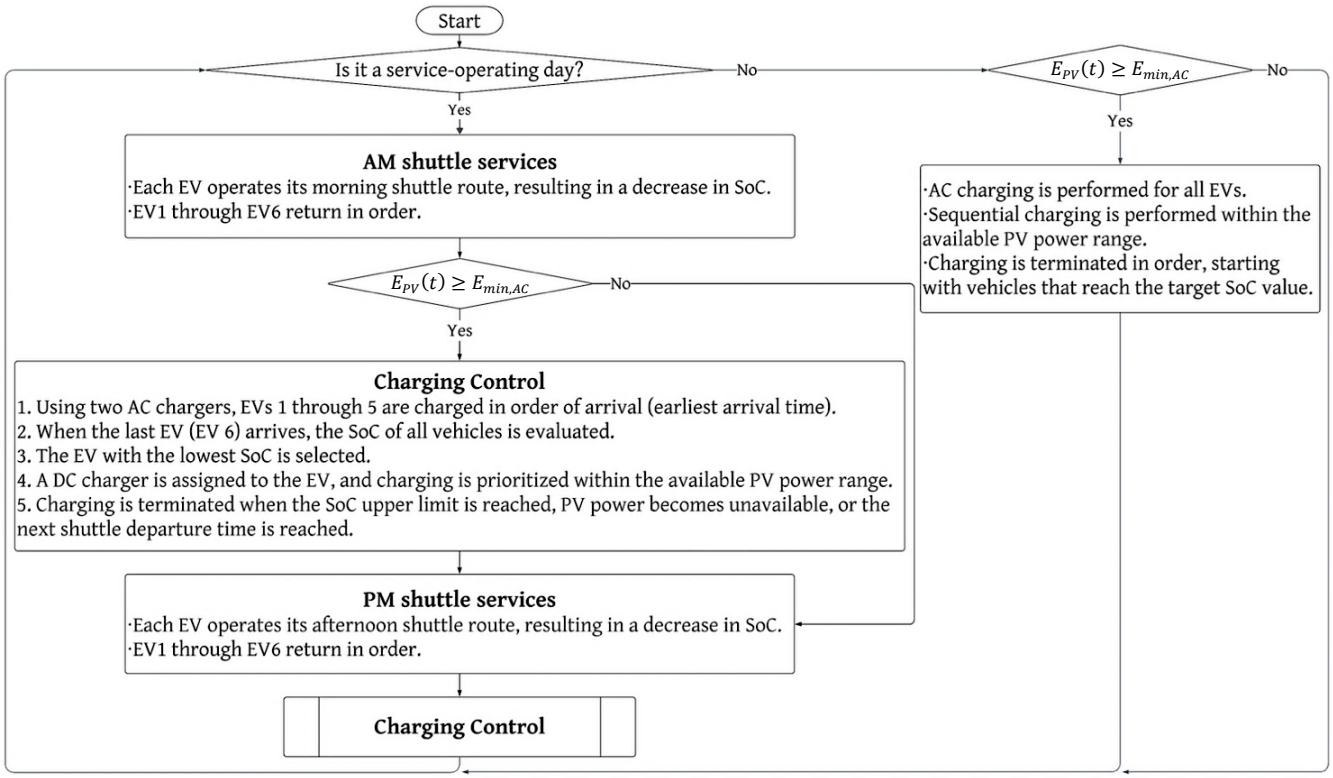

Fig. 3. Overview of the daily charging control logic based on PV availability and EV SoC.

Following the afternoon shuttle services, the same charging control procedure is applied. On non-service days, charging is performed only when the available PV energy exceeds the minimum AC threshold, and AC charging is executed sequentially for all EVs. Within each time step, however, the available PV energy is allocated simultaneously among the active chargers according to their rated power limits. In both cases, charging is terminated when the SoC upper limit is reached, PV energy becomes unavailable, or the next shuttle departure time is reached. At the end of each day, the final SoC values of all EVs are stored and used as the initial conditions for the subsequent day's simulation.

In the simulation, the charging control is executed with a fixed time step of Δt = 5 min. The PV availability at each step is treated as available energy $E_{PV}(t)$ [kWh], discretized from hourly PV energy data.

For AC charging, the minimum operating current requirement (6 A in IEC 61851-1) corresponds to P_{min} = 1.2 kW under a 200 V supply. This is implemented as an energy threshold $E_{min,AC} = P_{min,AC}\Delta t$ = 0.1 kWh per 5-min step. If the energy allocated to an AC charger after PV sharing falls below this threshold, charging is not activated during that time step.

When multiple chargers are simultaneously active, the available PV energy is shared equally among the active chargers and constrained by the rated power limits and SoC headroom of each charger. The SoC of all connected EVs is updated simultaneously within the same time step. The detailed charging control procedure is summarized in Algorithm 1.

Algorithm 1 Charging Control (Δt = 5 min)

for each time step t **do**
  Identify parked EVs
  Assign chargers:
   - AC chargers by arrival order
   - DC charger to EV with lowest SoC (if applicable)
  Determine available PV energy $E_{PV}(t)$
  Let N be the number of active chargers
  if $N > 0$ **then**
    Set provisional energy per charger $E_{share}(t)$
    $E_{share}(t) = E_{PV}(t) / N(t)$
  end if
  for each active charger c **do**
    Limit allocated energy by:
     (i) charger rating $P_{rated}(c)\Delta t$
     (ii) remaining SoC headroom
    If charger is AC and allocated energy $< E_{min,AC}$, set allocated energy = 0
  end for
  Update SoC of all connected EVs simultaneously
end for

The energy quantities used in Algorithm 1 are defined as follows. At each time step t, the available PV energy is denoted by $E_{PV}(t)$ [kWh], obtained from the discretized PV profile with Δt = 5 min. If $N(t)$ chargers are active at time step t, the provisional energy shared equally among them is

$$E_{share}(t) = \frac{E_{PV}(t)}{N(t)} \quad (1)$$

For each active charger c, the maximum admissible energy within the time step is constrained by both the charger rating and the remaining battery capacity up to the SoC upper bound:

$$E_{max}(c,t) = min\left(P_{rated}(c)\Delta t, \frac{(SoC_{max} - SoC_{i(t,c)})C_{battery}}{100}\right) \quad (2)$$

where $P_{rated}(c)$ [kW] is the rated power of charger c, $SoC_{i(t,c)}$ [%] is the current state of charge of the EV connected to charger c, and $C_{battery}$ [kWh] is the battery capacity.

The energy allocated to charger c is therefore

$$E_{alloc}(c,t) = min(E_{share}(t), E_{max}(c,t)) \quad (3)$$

For AC charging, a minimum operating threshold derived from IEC 61851-1 is applied. With $P_{min,AC}$ = 1.2 kW (6 A at 200 V), the minimum energy per time step is

$$E_{min,AC} = P_{min,AC}\Delta t \quad (4)$$

If $E_{alloc}(c,t) < E_{min,AC}$, AC charging is not activated during that time step. After determining $E_{alloc}(c,t)$ for all active chargers, the SoC of all connected EVs is updated simultaneously within the same time step using the allocated energy.

3.2. Algorithmic Procedure for PV Charging and SoC Computation

The charging process and the resulting variation in battery state-of-charge (SoC) are modeled through sequential calculations including PV energy generation, temperature correction, system losses, charging-path efficiency, and vehicle energy consumption. Since the Japan Meteorological Agency (JMA) provides hourly integrated solar radiation data, the PV output in this study is consistently treated as energy (kWh), rather than instantaneous power.

3.2.1. PV energy estimation

The hourly solar radiation provided by JMA, $g_h(t)$ [MJ/m²], represents the total incident solar energy per unit area during hour t. It is converted into kWh/m² as:

$$H_h(t) = g_h(t)c_{MJ} \quad (5)$$

where c_{MJ} = 0.27778 [kWh/MJ] is the unit conversion factor. The total active area of the PV array is expressed as

$$A = nS \quad (6)$$

where n is the number of PV modules and S [m²] is the area of a single module.

To account for temperature dependence, the PV cell temperature is estimated using the NOCT-based formulation consistent with the PVWatts model [27]:

$$T_c(t) = T_a(t) + \frac{NOCT-20}{800}G(t) \quad (7)$$

$$G(t) = \frac{H_h(t)1000}{3600} \quad (8)$$

where $T_a(t)$ [°C] is the ambient temperature and $G(t)$ [W/m²] is the hourly average radiation corresponding to $H_h(t)$. The Nominal Operating Cell Temperature was set to NOCT = 45°C, which is a representative value reported in crystalline silicon module datasheets [28].

The temperature-corrected DC-side PV energy can then be expressed as:

$$E_{DC}(t) = H_h(t)A\eta[1 + \gamma_P(T_c(t) - 25)] \quad (9)$$

where η is the module efficiency at standard test conditions, and γ_P = -0.004°C^{-1} is the temperature coefficient specified by the manufacturer [28].

3.2.2. System losses and time discretization

The usable AC-side PV energy is obtained by considering system-level losses, including inverter, wiring, mismatch, and soiling losses. It can be expressed as:

$$E_{AC}(t) = E_{DC}(t)\left(1 - L_{sys}\right) \quad (10)$$

where L_{sys} = 0.14 is adopted from the default assumption of the PVWatts model [28]. The quantity $E_{AC}(t)$ represents the available PV energy during hour t.

Since the EV charging simulation is performed at a 5-minute resolution, the hourly PV energy is equally distributed into twelve sub-intervals:

$$E_{5min}(t,k) = \frac{E_{AC}(t)}{12} \quad (11)$$

where k = 1, … ,12 represents the twelve 5-minute intervals within hour t. Thus, the charging model uses energy per 5-minute interval (kWh/5 min) as input. The energy available in each 5-min interval, $E_{5min}(t,k)$, represents the PV energy that can be utilized for EV charging during that interval.

To verify the plausibility of the PV generation model, the annual PV yield estimated in this study was compared with regional photovoltaic potential data obtained from the Renewable Energy Potential System (REPOS) published by the Ministry of the Environment of Japan [29]. For a PV system with a capacity of 140 kW, the annual PV generation calculated using the proposed model was 177,586.41 kWh for the year 2025. In comparison, the annual PV potential estimated from REPOS for the same capacity is approximately 187,840 kWh. The difference between the two estimates is approximately 5.5%, which is considered reasonable because the present model explicitly includes system loss factors and operational inefficiencies. Therefore, the estimated annual PV yield is in good agreement with the regional reference value, supporting the plausibility of the adopted PV generation model for the study site.

The actual charging energy delivered to each EV is determined according to the charging control procedure described in Algorithm 1.

3.2.3. Energy transferred to the EV battery

The energy charged to the EV battery during each interval depends on the charging-path efficiency. It can be expressed as:

$$E_{charge}(t,k) = \begin{cases} E_{5min}(t,k)\varepsilon_{AC}(AC\ charging) \\ E_{5min}(t,k)\varepsilon_{DC}(DC\ charging) \end{cases} \quad (12)$$

The efficiencies are defined as:

$$\varepsilon_{AC} = \eta_{inv}\eta_{line}\eta_{ac-dc}\eta_{batt} \quad (13)$$

$$\varepsilon_{DC} = \eta_{inv}\eta_{line}\eta_{batt} \quad (14)$$

where η_{inv} is the inverter efficiency, η_{line} is the indoor power transmission efficiency, η_{ac-dc} is the onboard AC-DC conversion efficiency applicable only to AC charging, and η_{batt} is the battery acceptance efficiency.

3.2.4. SoC variation

The increase in SoC due to PV charging is expressed as:

$$\Delta SoC_{charge}(t,k) = \frac{E_{charge}(t,k)}{C_{battery}} \times 100 \quad (15)$$

where $C_{battery}$ [kWh] is the nominal battery capacity.

The decrease in SoC during driving is calculated from GPS-based distance data as:

$$\Delta SoC_{drive}(t) = SoC_0 - \frac{E_{rate}d_t}{C_{battery}} \times 100 \quad (16)$$

where SoC_0 [%] is the initial state of charge at the beginning of the driving period, E_{rate} [kWh/km] is the vehicle energy consumption rate, and d_t [km] is the cumulative driving distance.

Finally, the SoC at time t is obtained as:

$$SoC(t) = SoC(t-1) - \Delta SoC_{drive}(t) + \Delta SoC_{charge}(t) \quad (17)$$

The SoC at time step t is obtained by subtracting the SoC decrease due to driving and adding the SoC increase due to PV charging to the previous state $SoC(t-1)$. The model is implemented with a discrete time step of 5 minutes, consistent with the charging simulation interval. The SoC is constrained within the operational bounds of the battery to prevent unrealistic overcharge or depletion.

In this study, the SoC variation during driving is not directly obtained from onboard vehicle logs. Instead, it is estimated from recorded driving distance using an assumed constant energy efficiency. Since this research aims to evaluate the feasibility of PV2V electrification, a simplified distance-based modeling approach is adopted. Therefore, the SoC used in this study represents a model-based estimated value rather than a directly measured operational SoC.

A representative vehicle energy efficiency of 6.0 km/kWh is adopted based on the manufacturer's catalog specifications for vehicles of a similar class. It should be noted that the model does not explicitly account for factors that can affect energy consumption in real driving conditions, such as ambient temperature, passenger load, stop-and-go traffic, or road

gradients. Accordingly, the estimated SoC values should be interpreted as approximate indicators of energy consumption under typical operating conditions rather than precise measurements of battery state. The objective of this study is not to reproduce the exact battery SoC but to evaluate charging feasibility under representative shuttle operation conditions.

4. Analysis of Charging Sequence

4.1. Percentile-Based Classification of Meteorological Conditions for Simulation

Japan has clear seasonal changes, including summer, winter, and transitional periods. In addition, weather phenomena such as the rainy season, frequent winter cloud cover, and typhoons affect solar radiation levels. As a result, PV generation conditions vary considerably throughout the year. Even during seasons generally considered favorable for solar energy, continuous cloud cover or rainfall can significantly reduce daily solar radiation.

If PV2V EV charging is evaluated directly using chronological meteorological data, the results may depend heavily on specific yearly fluctuations or short-term weather variations. This makes it difficult to clearly identify the fundamental relationship between PV energy supply and EV charging demand. To provide a clearer and more reproducible evaluation framework, meteorological conditions were classified into representative radiation levels based on the statistical distribution of observed data.

Figure 4 shows the relationship between daily solar radiation and daily sunshine duration based on meteorological data from the Japan Meteorological Agency (JMA) for the period 2020–2024. The horizontal axis represents daily solar radiation, and the vertical axis represents daily sunshine duration [h]. Each point corresponds to one day. Here, daily solar radiation refers to the total solar energy incident on a horizontal surface over one day [MJ/m^2].

A strong positive correlation was observed (r = 0.843), indicating that days with lower solar radiation generally correspond to shorter sunshine duration. Because solar radiation directly determines PV energy generation, it is used as the primary variable for meteorological classification. Sunshine duration is analyzed together with solar radiation to illustrate their empirical relationship and to provide a meteorological interpretation of the radiation categories.

Daily solar radiation R_d was classified using the empirical 25th and 75th percentiles of the dataset (2020–2024). The calculated threshold values were: Q_{25} = 9.8 MJ/m^2, Q_{75} = 20.4 MJ/m^2. Based on these thresholds, meteorological conditions were defined as:

- Low-radiation days : $R_d \leq Q_{25}$
- Normal-radiation days : $Q_{25} \leq R_d \leq Q_{75}$
- High-radiation days : $R_d \geq Q_{75}$

This percentile-based approach avoids assumptions about the underlying distribution and reflects the empirical radiation characteristics of the study region.

From a meteorological perspective, High-radiation days generally correspond to clear-sky conditions with sustained solar exposure and extended sunshine duration, representing favorable environments for PV generation. Normal-radiation days reflect intermediate conditions, such as partially cloudy or transitional weather states. In contrast, Low-radiation days are characterized by limited solar availability, typically associated with overcast skies, rainfall events (including the rainy season), winter cloud cover, or typhoon-related disturbances. Given the strong empirical relationship between radiation and sunshine duration, these categories reflect not only total daily PV energy potential but also the effective charging time window.

Among the three categories, the Low-radiation condition is particularly important for this study. Under such conditions, PV energy production decreases, the available charging window shortens, and the risk of insufficient state-of-charge increases. Therefore, evaluating whether EV shuttle operation remains feasible under Low-radiation conditions is essential for assessing the robustness of PV2V charging strategies. If feasibility can be maintained under Low-radiation condition, system performance under more favorable conditions can be reasonably expected.

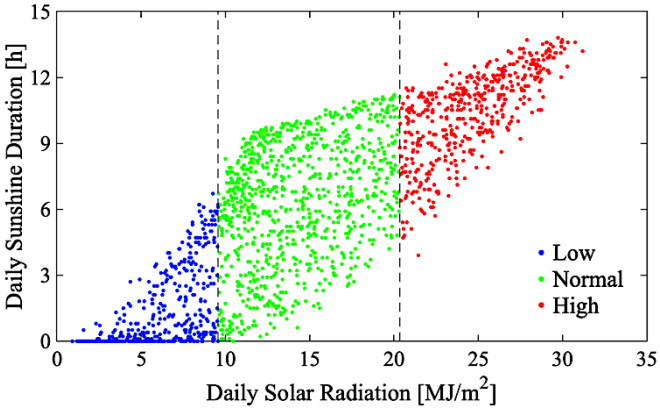

Fig. 4. Percentile-based categorization of daily solar radiation in relation to sunshine duration (2020–2024 dataset).

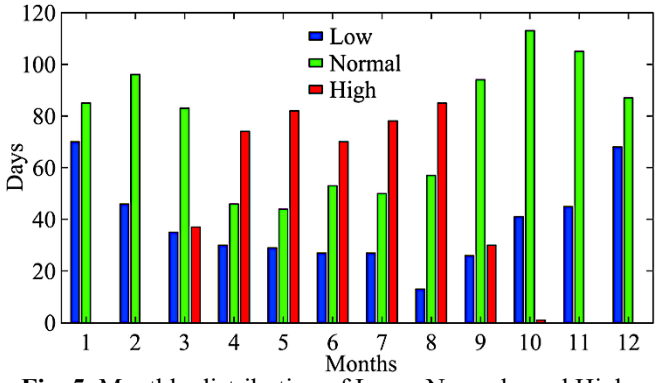

Fig. 5. Monthly distribution of Low-, Normal-, and High-radiation days based on the percentile-based classification (2020–2024 dataset).

Table 2. Monthly percentage distribution of radiation categories (2020–2024 dataset)

Month	*Low* (%)	*Normal* (%)	*High* (%)
1	15.3	9.3	0.0
2	10.0	10.5	0.0
3	7.6	9.0	8.1
4	6.5	5.0	16.1
5	6.3	4.8	17.9
6	5.9	5.8	15.3
7	5.9	5.4	17.0
8	2.8	6.2	18.6
9	5.6	10.3	6.5
10	8.9	12.3	0.2
11	9.8	11.5	0.0
12	14.8	9.5	0.0

Figure 5 shows the monthly distribution of the three radiation categories derived from the percentile-based classification. The bar chart indicates the number of days classified as Low-, Normal-, and High-radiation conditions for each month based on the 2020–2024 meteorological dataset. High-radiation days occur more frequently during summer months, reflecting stable clear-sky conditions with strong solar radiation. In contrast, Low-radiation days appear more often during winter months when solar radiation is reduced due to increased cloud cover and shorter daylight hours. Normal-radiation days are distributed across most months, representing intermediate meteorological conditions between these two extremes.

The monthly percentage distribution of each radiation category is summarized in Table 2. The table provides the quantitative proportion of Low-, Normal-, and High-radiation days for each month based on the 2020–2024 dataset. These numerical results support the seasonal tendencies observed in Fig. 5 and confirm that all radiation categories occur throughout the year, indicating that the percentile-based classification reflects the natural variability of solar radiation rather than strict seasonal boundaries.

Based on this percentile-based categorization, representative 28-day PV input profiles were constructed by randomly sampling daily radiation data within each category. The 28-day duration was selected to represent a typical monthly-scale operational period while maintaining consistency across different calendar months. This sampling approach preserves the natural day-to-day variability inherent in each radiation class, avoiding the artificial smoothing that would result from averaged profiles.

By generating multi-day sequences within the Low, Normal, and High categories, the model enables systematic evaluation of PV–EV operational feasibility under unfavorable, typical, and favorable meteorological conditions.

4.2. Simulation Setup

This section describes the main assumptions used in the simulation model. The specifications of the PV modules, vehicles, charging infrastructure, and power transfer efficiencies are summarized in Table 3.

Table 3. Summary of simulation assumptions

Category	*Parameter*	*Value*	*Description*
Power system	Grid connection	None	EV charging is supplied only by PV
	Energy storage system (ESS)	None	No stationary storage system
PV module	Module type	SHARP NQ-254BM	Crystalline silicon module
	Rated output	254 W	Manufacturer specification
	Module conversion efficiency	19%	PV module efficiency
Vehicle model	Vehicle type	Nissan e-NV200	Shuttle vehicle
	Battery capacity	40 kWh	Lithium-ion battery
	Initial SoC	90%	Start of simulation
	Energy efficiency	6.0 km/kWh	Assumed constant
SoC constraints	Minimum SoC	10%	Battery protection limit
	Maximum SoC	90%	Charging upper limit
Charging infrastructure	AC charger type	ELSEEV public Mode 3	AC charging
	AC charger power	6 kW	30 A, 200 V
	DC charger type	HFR1-30B9 (CHAdeMO Ver.2.0)	DC charging
	DC charger power	30 kW	75 A, 150–450 V
	Number of chargers	3 units	Two AC chargers and one DC charger
Power conversion efficiency	Inverter efficiency (η_{inv})	0.96	DC–AC conversion
	Line efficiency (η_{line})	0.98	Distribution loss
	AC–DC efficiency (η_{ac-dc})	0.93	On-board charger
	Battery efficiency (η_{batt})	0.97	Charging loss
Simulation settings	Time step	5 min	Simulation resolution

The simulation assumes six EVs operating shuttle services and charged using both AC and DC chargers. A total of three chargers are assumed for the six EVs, corresponding to approximately one charger per two vehicles. The operational SoC range is limited to 10–90% to mitigate battery degradation. The overall power transfer efficiency from the PV system to the EV battery is calculated based on component efficiencies, including inverter efficiency, line efficiency, charger efficiency, and battery charging efficiency.

In the analysis, the PV rated capacity was varied in increments of 1 kW, and simulations were repeated while adjusting the PV capacity so that the SoC of all EVs remained above the minimum SoC threshold during the simulation period. The smallest PV capacity satisfying this condition was defined as the required PV capacity.

4.3. Simulation Results

Figure 6 shows the one-month SoC transitions of all EVs under Low-radiation conditions, together with the corresponding PV generation profile, assuming a PV capacity of 248 kW. The top panel presents the PV energy per time step (E_{5min} [kWh]), while the lower panels show the SoC variations of EV1–EV6 over the simulation period. As shown in the figure, EV4 and EV5 exhibit more pronounced SoC reductions than the other vehicles because they experience higher shuttle operation loads and have shorter available charging time due to their later return times. In contrast, EV1–EV3 and EV6 maintain relatively stable SoC levels throughout the simulation period, indicating that sufficient charging opportunities are secured for these vehicles even under low solar conditions.

This result indicates that, under the current routing, EVs assigned longer daily driving distances are more susceptible to SoC depletion, whereas sufficient PV capacity enables the remaining EVs to sustain stable operation over the one-month period.

Figure 7 shows the one-month SoC transitions of all EVs under Normal-radiation conditions, together with the corresponding PV generation profile. The top panel presents the PV energy generated per 5-min time step (E_{5min} [kWh]), while the lower panels show the SoC variations of EV1–EV6 over the simulation period. With a PV capacity of 84 kW, all EVs maintain their SoC within the operational range throughout the simulation period. In particular, even EV4 and EV5, which operate relatively long shuttle routes, avoid critical SoC depletion under normal solar conditions.

This result indicates that a moderate PV capacity well below 140 kW, which represents a realistic installation scale for clinic facilities, is sufficient to sustain stable EV operation over a one-month period under typical solar conditions.

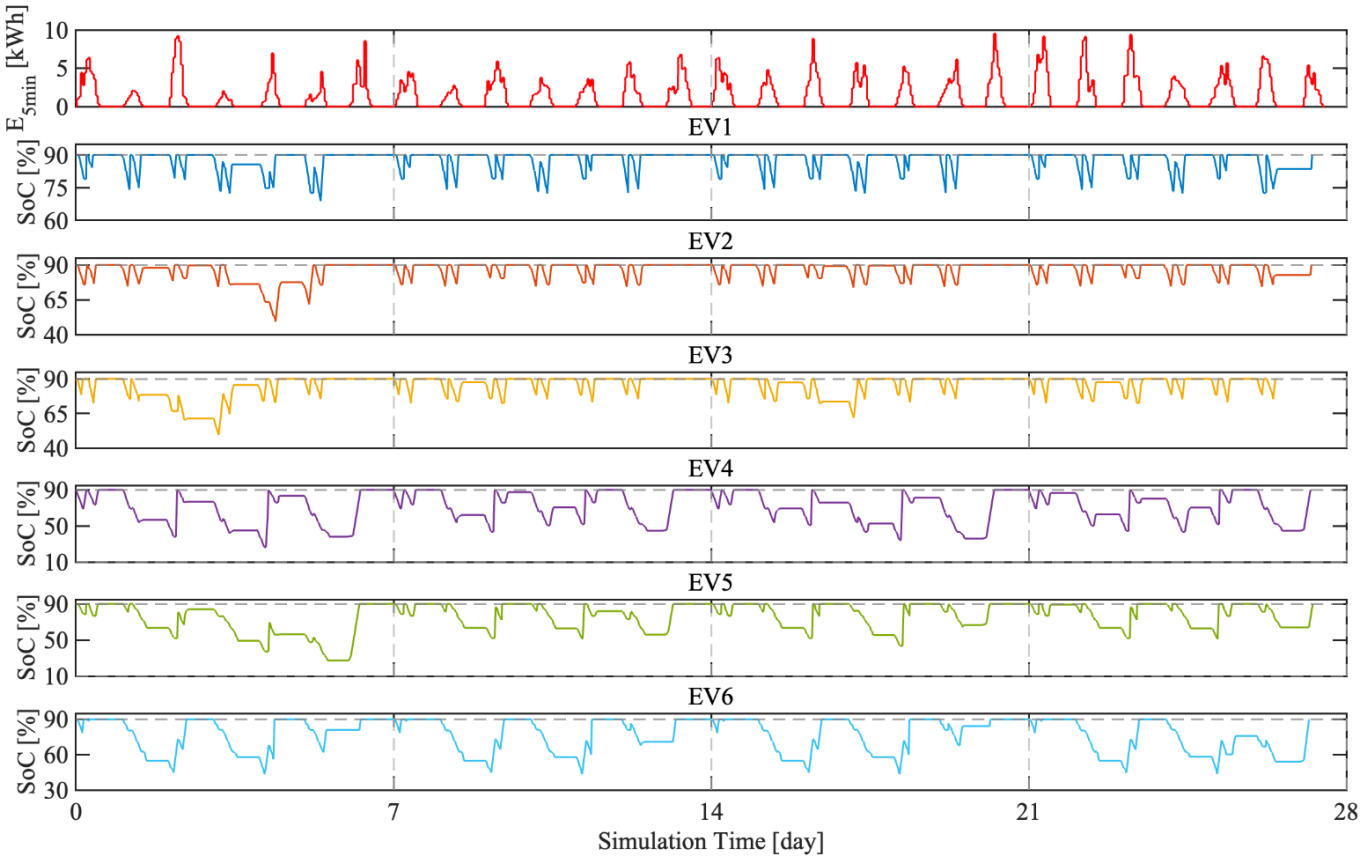

Fig. 6. SoC transitions over one month under Low-radiation conditions with a 248 kW PV system.

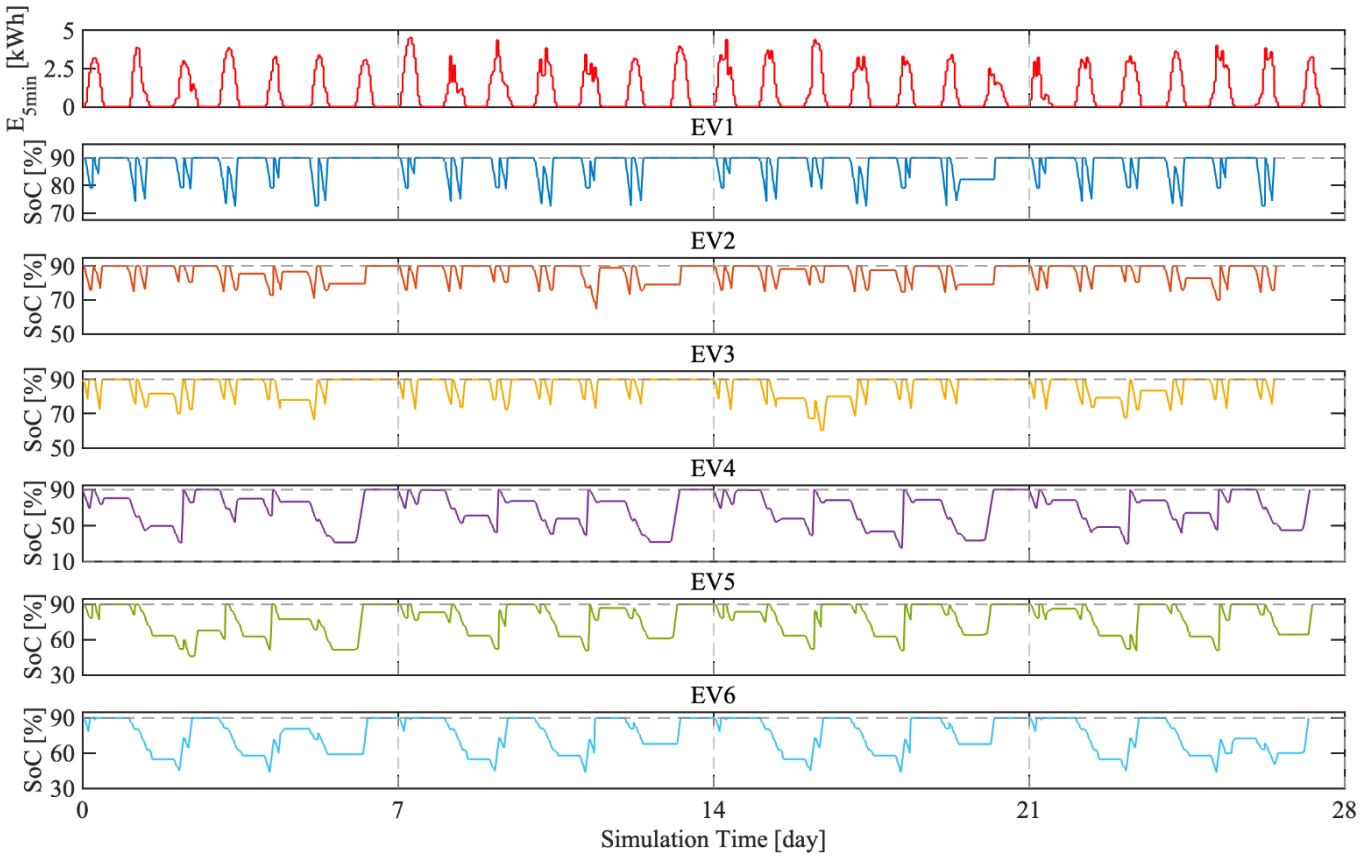

Fig. 7. SoC transitions over one month under Normal-radiation conditions with an 84 kW PV system.

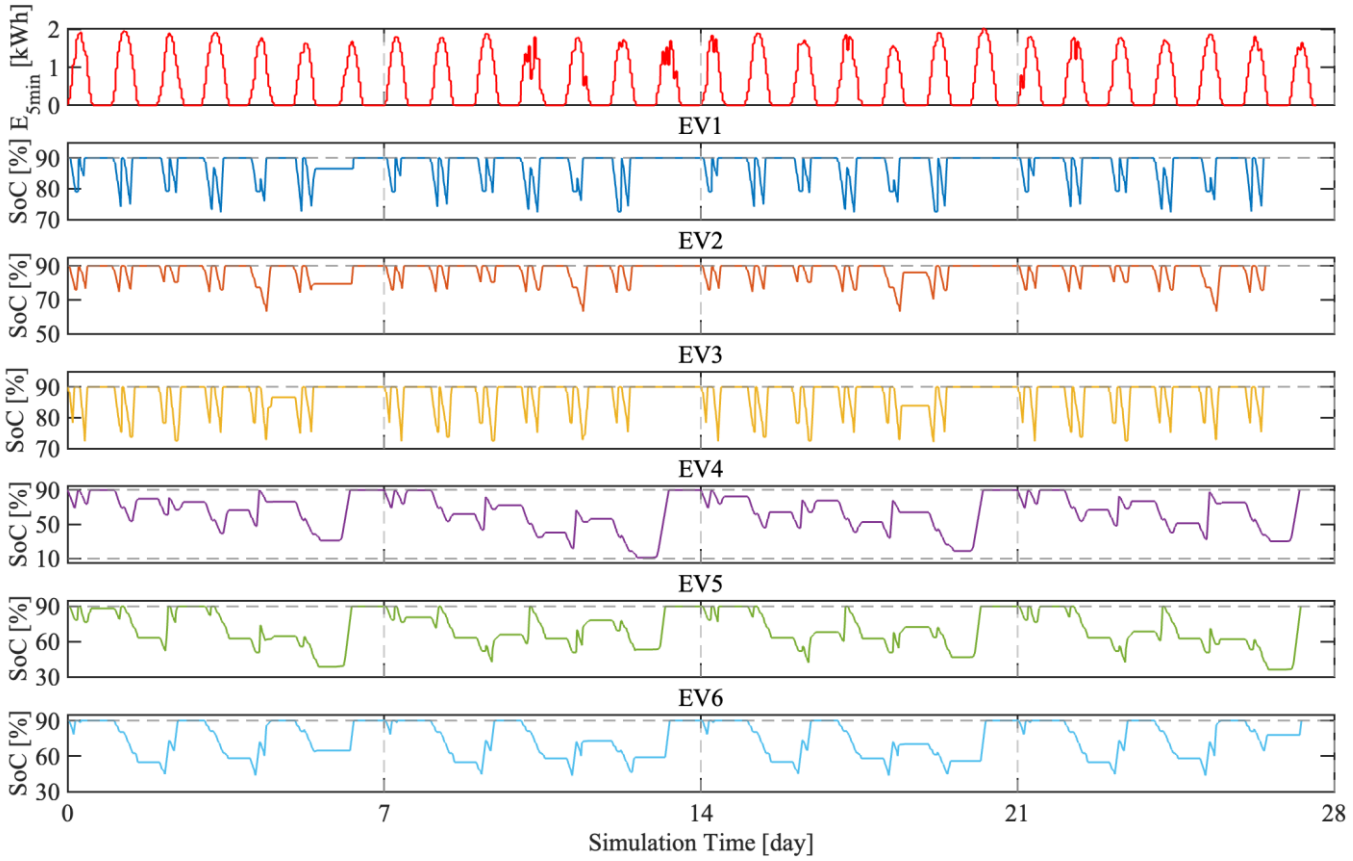

Fig. 8. SoC transitions over one month under High-radiation conditions with a 31 kW PV system.

Figure 8 shows the one-month SoC transitions of all EVs under High-radiation conditions, together with the corresponding PV generation profile. The top panel presents the PV energy generated per 5-min time step (E_{5min} [kWh]), while the lower panels show the SoC variations of EV1–EV6 over the simulation period. With a PV capacity of only 31 kW, all EVs maintain their SoC within the operational range throughout the simulation period. Even EV4 and EV5, which operate relatively long shuttle routes, do not reach critically low SoC levels under high solar conditions.

This result indicates that under favorable meteorological conditions, a relatively small PV system is sufficient to sustain stable EV shuttle operation, highlighting the strong dependence of the required PV capacity on solar conditions. These results collectively indicate that the PV capacity required to sustain EV shuttle operation strongly depends on solar radiation conditions. As solar conditions improve from Low to High radiation conditions, the required PV capacity decreases substantially, while EVs assigned to longer shuttle routes consistently lead to higher PV capacity requirements across all meteorological conditions.

5. Discussions

5.1. Reduction in Required PV Capacity Through Shuttle Route Reassignment Among EVs

The main analysis in this study evaluates PV capacity requirements under the current shuttle operation, where six EVs follow fixed routes. However, the simulation results indicate that insufficient charging time is a major limiting factor in PV2V charging. This limitation primarily arises from the imbalance in shuttle operation loads among EVs, as the assigned routes differ significantly in driving distance. Vehicles assigned longer routes experience larger SoC reductions during driving and tend to return later, which further reduces the time available for charging. As a result, these vehicles may not receive sufficient charging to maintain their SoC within the desired operational range. To investigate whether this limitation can be alleviated through operational adjustments, an additional simulation with route reassignment is examined in this discussion. The purpose is to clarify how reducing differences in driving distance among EVs affects the required PV capacity.

In this analysis, three shuttle operation patterns are considered, as summarized in Tables 4–6. In these tables, Day 1–Day 6 denote sequential operating days within a week (corresponding to Monday through Saturday), indexed to represent generalized daily operations in the simulation. The leftmost column indicates the EV identifier (EV1–EV6), and each table entry represents the shuttle route assigned to a specific EV on a given operating day.

The notation $EV_{i\text{-}j}$ denotes the route operated by vehicle EV i on Day j; for example, $EV_{1\text{-}1}$ represents the route operated by EV1 on Day 1 (Monday). Pattern I represents the current operation with fixed shuttle routes. Pattern II corresponds to a daily rotation of routes among EVs, in which assignments are exchanged without considering driving-distance differences. Pattern III represents a distance-aware reassignment strategy, where weekly driving distances are first calculated for all EVs, and vehicles with long and short distances are identified and paired so that shuttle routes are exchanged on a daily basis to reduce distance imbalance across the fleet.

Table 4. Shuttle route assignment under fixed-route operation (Pattern I)

EV	Day 1 *Mon.*	Day 2 *Tues.*	Day 3 *Wed.*	Day 4 *Thurs.*	Day 5 *Fri.*	Day 6 *Sat.*
EV1	$EV_{1\text{-}1}$	$EV_{1\text{-}2}$	$EV_{1\text{-}3}$	$EV_{1\text{-}4}$	$EV_{1\text{-}5}$	$EV_{1\text{-}6}$
EV2	$EV_{2\text{-}1}$	$EV_{2\text{-}2}$	$EV_{2\text{-}3}$	$EV_{2\text{-}4}$	$EV_{2\text{-}5}$	$EV_{2\text{-}6}$
EV3	$EV_{3\text{-}1}$	$EV_{3\text{-}2}$	$EV_{3\text{-}3}$	$EV_{3\text{-}4}$	$EV_{3\text{-}5}$	$EV_{3\text{-}6}$
EV4	$EV_{4\text{-}1}$	$EV_{4\text{-}2}$	$EV_{4\text{-}3}$	$EV_{4\text{-}4}$	$EV_{4\text{-}5}$	$EV_{4\text{-}6}$
EV5	$EV_{5\text{-}1}$	$EV_{5\text{-}2}$	$EV_{5\text{-}3}$	$EV_{5\text{-}4}$	$EV_{5\text{-}5}$	$EV_{5\text{-}6}$
EV6	$EV_{6\text{-}1}$	$EV_{6\text{-}2}$	$EV_{6\text{-}3}$	$EV_{6\text{-}4}$	$EV_{6\text{-}5}$	$EV_{6\text{-}6}$

Table 5. Shuttle route assignment with daily rotation (Pattern II)

EV	Day 1 *Mon.*	Day 2 *Tues.*	Day 3 *Wed.*	Day 4 *Thurs.*	Day 5 *Fri.*	Day 6 *Sat.*
EV1	$EV_{1\text{-}1}$	$EV_{2\text{-}2}$	$EV_{3\text{-}3}$	$EV_{4\text{-}4}$	$EV_{5\text{-}5}$	$EV_{6\text{-}6}$
EV2	$EV_{2\text{-}1}$	$EV_{3\text{-}2}$	$EV_{4\text{-}3}$	$EV_{5\text{-}4}$	$EV_{6\text{-}5}$	$EV_{1\text{-}6}$
EV3	$EV_{3\text{-}1}$	$EV_{4\text{-}2}$	$EV_{5\text{-}3}$	$EV_{6\text{-}4}$	$EV_{1\text{-}5}$	$EV_{2\text{-}6}$
EV4	$EV_{4\text{-}1}$	$EV_{5\text{-}2}$	$EV_{6\text{-}3}$	$EV_{1\text{-}4}$	$EV_{2\text{-}5}$	$EV_{3\text{-}6}$
EV5	$EV_{5\text{-}1}$	$EV_{6\text{-}2}$	$EV_{1\text{-}3}$	$EV_{2\text{-}4}$	$EV_{3\text{-}5}$	$EV_{4\text{-}6}$
EV6	$EV_{6\text{-}1}$	$EV_{1\text{-}2}$	$EV_{2\text{-}3}$	$EV_{3\text{-}4}$	$EV_{4\text{-}5}$	$EV_{5\text{-}6}$

Table 6. Shuttle route assignment with distance-balanced reassignment (Pattern III)

EV	Day 1 *Mon.*	Day 2 *Tues.*	Day 3 *Wed.*	Day 4 *Thurs.*	Day 5 *Fri.*	Day 6 *Sat.*
EV1	$EV_{1\text{-}1}$	$EV_{4\text{-}2}$	$EV_{1\text{-}3}$	$EV_{4\text{-}4}$	$EV_{1\text{-}5}$	$EV_{4\text{-}6}$
EV2	$EV_{2\text{-}1}$	$EV_{3\text{-}2}$	$EV_{2\text{-}3}$	$EV_{3\text{-}4}$	$EV_{2\text{-}5}$	$EV_{3\text{-}6}$
EV3	$EV_{3\text{-}1}$	$EV_{2\text{-}2}$	$EV_{3\text{-}3}$	$EV_{2\text{-}4}$	$EV_{3\text{-}5}$	$EV_{2\text{-}6}$
EV4	$EV_{4\text{-}1}$	$EV_{1\text{-}2}$	$EV_{4\text{-}3}$	$EV_{1\text{-}4}$	$EV_{4\text{-}5}$	$EV_{1\text{-}6}$
EV5	$EV_{5\text{-}1}$	$EV_{6\text{-}2}$	$EV_{5\text{-}3}$	$EV_{6\text{-}4}$	$EV_{5\text{-}5}$	$EV_{6\text{-}6}$
EV6	$EV_{6\text{-}1}$	$EV_{5\text{-}2}$	$EV_{6\text{-}3}$	$EV_{5\text{-}4}$	$EV_{6\text{-}5}$	$EV_{5\text{-}6}$

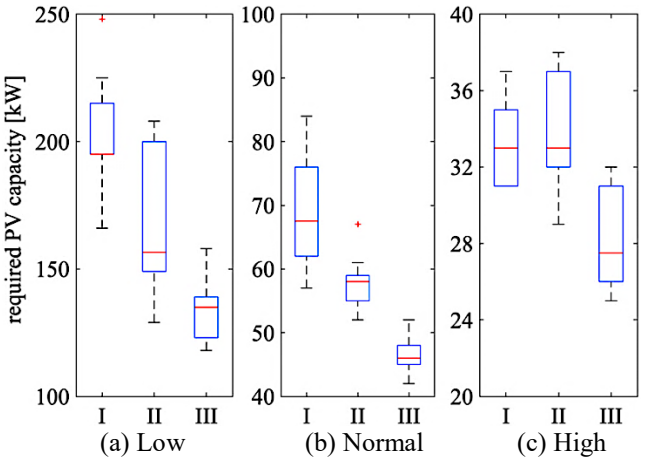

Fig. 9. Comparison of required PV capacity among shuttle route assignment patterns (Patterns I–III) under classified solar radiation conditions: (a) Low, (b) Normal, and (c) High.

In this analysis, route reassignment is performed under the assumption that the total daily driving distance of the EV fleet remains unchanged, thereby preserving the clinic's actual shuttle service demand. The evaluation is conducted using the same statistically classified meteorological conditions (Low, Normal, and High) defined in Section IV. The number of EVs is fixed at six, reflecting the actual operating condition of the clinic. For each weather category, multiple one-month PV patterns are simulated, and the minimum PV capacity required to keep all EVs within the SoC range of 10–90% is obtained.

Figure 9 shows a comparison of the minimum required PV capacity under three shuttle route assignment patterns (Patterns I–III) across different meteorological conditions. The vertical axis represents required PV capacity [kW], and each boxplot summarizes the results of one-month simulations. For each meteorological category, $N = 10$ paired one-month PV sequences were used as input to the charging simulations. Statistical differences among shuttle operation patterns were evaluated using the Wilcoxon signed-rank test with Holm correction ($\alpha = 0.05$). The detailed statistical results, including p-values and effect sizes, are summarized in Table 7.

For all meteorological categories, route reassignment reduces the required PV capacity compared with the fixed-route operation, indicating that operational modification itself improves PV2V charging feasibility. Comparing the reassignment patterns, both Pattern II and Pattern III show lower required PV capacities than Pattern I, confirming the effectiveness of route modification. The statistical analysis further supports this trend. Under Low and Normal radiation conditions, all pairwise comparisons among Patterns I–III were statistically significant ($p < 0.05$), with effect sizes (r) ranging from approximately 0.66 to 0.89, indicating moderate to large practical effects. In contrast, under High-radiation conditions the difference between Patterns I and II was not statistically significant, although Pattern III remained significantly lower than both Patterns I and II. The effect sizes observed under High conditions were generally smaller than those under Low and Normal conditions.

However, the reduction achieved by Pattern II remains limited. Because this pattern applies a simple daily rotation without considering differences in driving distance, it mainly redistributes variability among EVs and does not substantially increase effective charging time.

Table 7. Statistical comparison of shuttle operation patterns (Wilcoxon signed-rank test with Holm correction)

Weather condition	*Comparison* (Pattern)	*N*	*p*-values (Holm corrected)	*Effect size r*
Low	I vs II	10	0.031	0.66
	I vs III	10	0.006	0.89
	II vs III	10	0.023	0.77
Normal	I vs II	10	0.006	0.89
	I vs III	10	0.006	0.89
	II vs III	10	0.006	0.89
High	I vs II	10	0.594	0.02
	I vs III	10	0.012	0.89
	II vs III	10	0.016	0.89

In contrast, Pattern III, which pairs long and short driving-distance routes and alternates them daily, achieves a substantially larger reduction in the required PV capacity. Under Low-radiation conditions, where PV energy generation is most constrained, the required PV capacity is reduced by approximately 31% compared with the fixed-route operation. Specifically, the median required PV capacity is 135 kW, while the upper quartile is 139 kW, indicating that most simulation results fall within a range close to the realistically installable PV capacity of the facility (140 kW). Although a small number of cases exceed this capacity threshold, reaching up to 158 kW, the overall distribution remains concentrated around values near or below the assumed installation capacity.

These results indicate that balancing driving distances among vehicles is essential for reducing excessive SoC reductions and mitigating differences in vehicle return times. When certain EVs are repeatedly assigned longer routes, their batteries experience larger SoC decreases and they tend to return later, making it more difficult to secure sufficient charging time for maintaining the desired SoC level. By redistributing shuttle routes to reduce these imbalances, the charging time available to each vehicle becomes more evenly distributed, which contributes to more stable SoC trajectories across the fleet. The findings demonstrate that the sustainability of PV2V EV operation depends not only on the total PV energy available but also on the operational distribution of driving loads among vehicles. While simple route rotation provides only limited improvement, distance-balanced route reassignment enables more effective utilization of the available charging opportunities and contributes to reducing the required PV capacity.

5.2. Basis for PV Capacity Reduction through Shuttle Route Reassignment

To clarify the basis for the reduction in required PV capacity discussed in Section 5.1, the distribution of driving distances among EVs under different route assignment patterns is first examined. Table 8 summarizes the weekly shuttle driving distances assigned to each EV under the three route assignment patterns. The values represent the total driving distance [km] of each EV per day, including both the morning and afternoon shuttle services. For each pattern, the table reports the daily distances over one week as well as the total and mean distance assigned to each EV. To evaluate the degree of distance imbalance among EVs, the standard deviation (SD) of the mean driving distances was calculated for each pattern. The SD values were 10.63 km for Pattern I, 4.61 km for Pattern II, and 5.68 km for Pattern III, indicating that the imbalance in driving distance among EVs was significantly reduced when the shuttle route assignment pattern was changed from Pattern I to Patterns II and III.

Under Pattern I, certain EVs are repeatedly assigned longer shuttle routes while others are assigned shorter routes, resulting in an uneven distribution of driving distances among vehicles. Because longer driving distances correspond to larger energy consumption, such an imbalance increases the likelihood that specific EVs experience excessive SoC depletion. Route reassignment in Patterns II and III reduces this imbalance by redistributing shuttle routes among EVs. In

Pattern II, routes are rotated among vehicles on a daily basis, which partially mitigates the concentration of long-distance routes on particular EVs. Pattern III further improves this balance by pairing long-distance and short-distance routes and alternating them among EVs.

As visualized in the heatmap of Table 8, Pattern III reduces the occurrence of consecutive long-distance assignments for the same EV compared with Pattern II. Avoiding consecutive long-distance operations is particularly important for maintaining stable SoC levels. When an EV repeatedly operates long-distance routes on consecutive days, the daily SoC reduction caused by the long driving distance may not be fully recovered through the available charging opportunity between shuttle services. As a result, the SoC gradually decreases over successive days. In such cases, a larger PV capacity would be required to sufficiently recover the SoC within the limited charging window. By contrast, distributing long and short routes more evenly among EVs helps prevent excessive SoC depletion and stabilizes charging requirements.

This operational balancing directly contributes to improving charging-time availability and maintaining stable SoC levels across the fleet. As a result, the PV capacity required to sustain EV operation can be reduced. It should also be noted that the total daily shuttle demand remains unchanged across all patterns. Because route reassignment only changes the combination of routes assigned to each EV within a day, the total driving distance per day is identical for all patterns. Consequently, the weekly total and average distances remain the same, ensuring that the comparison among patterns is conducted under identical service-demand constraints.

These operational differences in route assignment directly influence the return timing of EVs and the availability of charging opportunities. To further understand how these differences affect the charging process, Figure 10 illustrates the temporal distribution of PV generation and its utilization for EV charging during a representative day under three shuttle operation patterns: (a) Pattern I, (b) Pattern II, and (c) Pattern III. The horizontal axis represents the time of day, and the vertical axis represents energy per simulation time step [kWh/5 min].

In each panel, the red line indicates the PV energy generated at each 5-minute simulation time step. The green shaded area represents the portion of PV energy consumed for EV charging, while the blue line shows the remaining PV energy that is not used for charging. By comparing panels (a)–(c), the figure visualizes how the temporal distribution of PV consumption changes depending on the shuttle route assignment pattern. It is also worth noting that, on the representative day shown in Fig. 10(c) for Pattern III, the total PV generation is approximately 316 kWh, of which about 82 kWh (approximately 26%) is utilized for EV charging, leaving roughly 233 kWh (approximately 74%) as surplus PV energy. This indicates that a large portion of PV energy remains unused during daytime operation.

Under Pattern I, EVs assigned to longer shuttle routes tend to return later to the facility and experience larger SoC reductions. Because the departure time for the afternoon shuttle service is determined by the patients' treatment completion time and does not differ significantly among vehicles, a later return results in a shorter charging window before the next departure. Consequently, charging for these EVs begins relatively late, resulting in a rightward shift in the temporal distribution of PV energy consumption.

Table 8. Actual driving distances of shuttle EVs during the morning shuttle routes under three operation patterns

Pattern	*EV route*	Day 1 *Mon.*	Day 2 *Tues.*	Day 3 *Wed.*	Day 4 *Thurs.*	Day 5 *Fri.*	Day 6 *Sat.*	*Total* [km]	*Mean* [km]
Pattern I	EV1	40.66	75.54	53.27	75.61	43.98	79.64	368.7	61.5
	EV2	66.36	70.43	46.02	71.11	64.8	72.64	391.36	65.2
	EV3	70.43	74.31	69.84	64.16	69.4	63.76	411.9	68.7
	EV4	90.25	89.51	79.12	89.14	78.63	113.74	540.39	90.1
	EV5	59.58	86.19	61.02	84.18	60.86	82.45	434.28	72.4
	EV6	35.49	85.44	45.95	76.02	64.11	66.73	373.74	62.3
	Total	362.77	481.42	355.22	460.22	381.78	478.96	2520.37	70.0
Pattern II	EV1	40.66	70.43	69.84	89.14	60.86	66.73	397.66	66.3
	EV2	66.36	74.31	79.12	84.18	64.11	79.64	447.72	74.6
	EV3	70.43	89.51	61.02	76.02	43.98	72.64	413.6	68.9
	EV4	90.25	86.19	45.95	75.61	64.8	63.76	426.56	71.1
	EV5	59.58	85.44	53.27	71.11	69.4	113.74	452.54	75.4
	EV6	35.49	75.54	46.02	64.16	78.63	82.45	382.29	63.7
	Total	362.77	481.42	355.22	460.22	381.78	478.96	2520.37	70.0
Pattern III	EV1	40.66	89.51	53.27	89.14	43.98	113.74	430.3	71.7
	EV2	66.36	74.31	46.02	64.16	64.8	63.76	379.41	63.2
	EV3	70.43	70.43	69.84	71.11	69.4	72.64	423.85	70.6
	EV4	90.25	75.54	79.12	75.61	78.63	79.64	478.79	79.8
	EV5	59.58	85.44	61.02	76.02	60.86	66.73	409.65	68.3
	EV6	35.49	86.19	45.95	84.18	64.11	82.45	398.37	66.4
	Total	362.77	481.42	355.22	460.22	381.78	478.96	2520.37	70.0

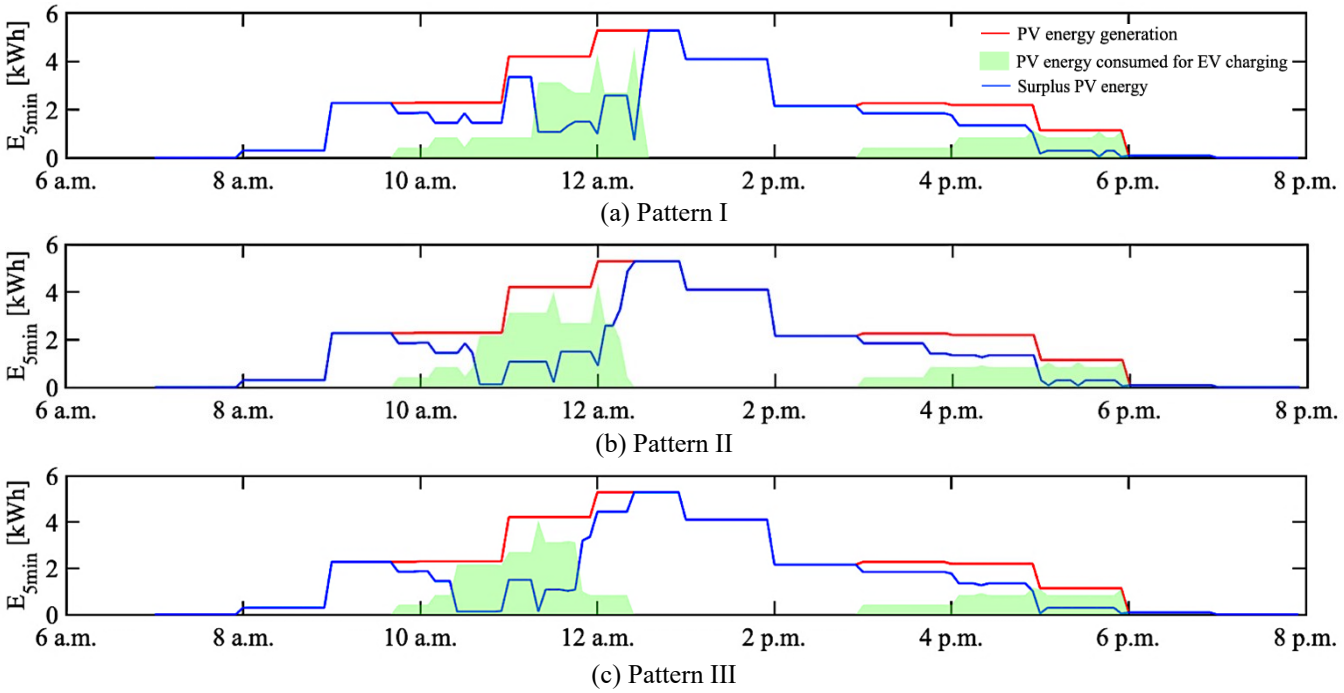

(a) Pattern I

(b) Pattern II

(c) Pattern III

Fig. 10. Temporal shift in PV consumption under different shuttle operation patterns.

After route reassignment, the return times of EVs become more balanced compared with Pattern I. In Pattern II, shuttle routes are rotated among EVs on a daily basis, which partially redistributes the driving-distance imbalance. As a result, some EVs assigned to longer routes in Pattern I return slightly earlier, allowing charging to start somewhat earlier and shifting the PV consumption distribution slightly toward earlier hours. In Pattern III, long and short driving-distance routes are explicitly paired and alternated among EVs. Because EVs assigned to longer routes are paired with shorter routes on alternating days, the EV that experiences the largest SoC reduction can return earlier than in Pattern I. This allows charging to start earlier for the EV that requires the largest SoC recovery, shifting the PV consumption toward earlier hours. As observed in Fig. 10, the green shaded PV consumption area gradually shifts leftward from Pattern I to Pattern III.

By enabling earlier charging for EVs with larger SoC reductions, route reassignment improves charging-time availability and suppresses excessive SoC depletion. Consequently, adequate SoC levels can be maintained without requiring additional PV capacity. This discussion further highlights that PV capacity requirements are influenced not only by meteorological conditions but also by operational design. While increasing PV capacity is one possible solution, appropriate route reassignment provides a practical alternative that improves charging feasibility without additional infrastructure. By combining statistically representative PV conditions with simple yet targeted operational adjustments, such as balancing shuttle routes according to driving distance, PV2V EV charging systems can be designed more efficiently and realistically. This approach provides a practical and cost-effective strategy for healthcare facilities seeking to operate EV shuttle services sustainably under constrained solar conditions.

5.3. Sensitivity Analysis of the Simulation Model

To evaluate the robustness of the simulation results, a sensitivity analysis was conducted by modifying key operational efficiencies and system conditions, including PV output, vehicle energy consumption, charging efficiency, and SoC operating range. The parameter settings for the Best-case and Worst-case scenarios are summarized in Table 9. As a representative case, the simulation was performed under the Low solar radiation condition using Pattern III, which showed the highest PV utilization efficiency among the route assignment strategies.

In the Best-case scenario, where vehicle energy consumption decreases and charging efficiency improves, the required PV capacity was reduced to 93 kW. In contrast, in the Worst-case scenario, where PV output decreases and vehicle energy consumption increases, the required PV capacity increased to 303 kW.

These results indicate that the required PV capacity is sensitive to system parameters such as vehicle energy consumption and charging efficiency. In particular, the deterioration of vehicle energy efficiency had a significant impact on the required PV capacity, leading to a substantial increase in the PV capacity required to sustain EV operation.

Recent studies have explored advanced optimization and control techniques for photovoltaic systems and renewable microgrids, including intelligent MPPT control, reliability-conscious power flow optimization, and machine-learning-based solar radiation estimation [30–32]. These technological developments may further support the efficient operation of PV-powered EV charging systems when combined with the operational strategies examined in this study.

Table 9. Parameters used in the sensitivity analysis

Parameter	*Best-case*	*Worst-case*
PV output factor	0%	-10%
Driving energy consumption	-15%	+15%
Charging efficiency	0%	-5%
SoC operating range	10-90%	20-90%

6. Conclusion

This study evaluated the feasibility of operating clinic shuttle services using EVs powered solely by PV systems, with a focus on determining the required PV capacity under realistic operational and meteorological conditions. Using actual driving records from a dialysis clinic in Japan, month-long charging simulations were conducted based on statistically classified solar conditions. The key findings of this study are summarized as follows:

1) By statistically analyzing the relationship between solar radiation and sunshine duration, meteorological conditions were classified into three representative categories (Low, Normal, and High). This classification enabled the construction of PV input profiles that capture typical solar characteristics while excluding irregular and unrepresentative fluctuations, leading to more interpretable charging simulations.

2) Under fixed shuttle routes, the imbalance in driving distances among EVs results in larger SoC reductions for vehicles assigned to longer routes. These vehicles also tend to return later, which reduces the time available for charging and makes it difficult to secure sufficient charging to maintain the desired SoC level, particularly under low-solar conditions. Consequently, PV capacity requirements may be overestimated when such operational constraints are not explicitly considered.

3) A simple operational adjustment based on shuttle route reassignment was introduced to reduce driving-distance imbalance among EVs and improve charging-time availability. Under low-solar conditions, this approach reduced the required PV capacity by approximately 31% compared with fixed-route operation, without increasing the number of EVs or charging equipment.

These findings demonstrate that PV capacity requirements are influenced not only by meteorological conditions but also by operational design. While increasing PV capacity is one possible solution, improving operational flexibility—such as balancing driving distances among EVs—provides a cost-effective alternative for maintaining stable SoC levels. Overall, this study highlights that combining statistically representative PV conditions with practical operational strategies enables a more realistic evaluation of PV2V EV charging systems and supports the efficient design of sustainable EV shuttle services for healthcare facilities.

As future work, improving the sustainability of PV2V EV shuttle operation remains an important research direction. The sensitivity analysis indicates that under the most unfavorable conditions the required PV capacity can reach approximately 303 kW, which exceeds the practical PV installation limit of the facility. To address this issue, strategies for reducing the required PV capacity will be investigated, including the optimization of shuttle route assignments and the integration of battery energy storage systems (BESS). Because the simulation results show that surplus PV generation frequently occurs during daytime periods, storing this excess energy and utilizing it during periods of insufficient PV output may enable the required PV capacity to be reduced to a more practical level. In addition, economic analyses will be conducted to investigate the trade-off between PV capacity expansion and the operational benefits of EV electrification, such as reductions in patient transportation costs. By jointly considering energy infrastructure investment and operational cost savings, future studies will aim to identify optimal system configurations that balance technical feasibility with economic efficiency.

Acknowledgements

The authors would like to thank Miyamoto Clinic's medical staff for their cooperation and support in providing operational insights and contextual data essential for this study.

This work is supported by JSPS KAKENHI Grant Number JP24K07938.

Author Contributions

Koki Kumaoka was responsible for the conceptualization, validation, resources, data curation, software development, and project administration. Haru Morikawa, Nobumasa Matsui, Jiyoung Choi, and Yuji Mizuno jointly contributed to the methodology, formal analysis, investigation, original draft preparation, review and editing, visualization, supervision, and funding acquisition. All authors have read and agreed to the published version of the manuscript.

Conflict of Interest

The authors declared no potential conflicts of interest with respect to the research, authorship, and/or publication of this article.

References

[1] Council for the Promotion of Global Warming Countermeasures in Hospitals, "Low Carbon Society Action Plan for Hospitals: 2021 Follow-up Fact-Finding Survey Report," Tokyo, Japan, 2022.

[2] Council for the Promotion of Global Warming Countermeasures in Hospitals, "Low Carbon Society Action Plan for Hospitals: 2023 Follow-up Fact-Finding Survey Report," Tokyo, Japan, 2024.

[3] M. M. R. Ahmed, S. Mirsaeidi, M. A. Koondhar, N. Karami, E. M. Tag-Eldin, N. A. Ghamry, R. A. El-Sehiemy, Z. M. Alaas, I. Mahariq, and A. M. Sharaf, "Mitigating uncertainty problems of renewable energy resources through efficient integration of hybrid solar PV/wind systems into power networks," IEEE Access, vol. 12, pp. 30311–30328, 2024.

[4] A. Al Hadi, C. A. Santos Silva, E. Hossain, and R. Challoo, "Algorithm for demand response to maximize the penetration of renewable energy," IEEE Access, vol. 8, pp. 55279–55288, 2020.

[5] Agency for Natural Resources and Energy, "Annual Report on Energy 2023 (Energy White Paper 2024)," Ministry of Economy, Trade and Industry, Tokyo, Japan, June 2024.

[6] Y. Mizuno, M. Tanaka, Y. Tanaka, F. Kurokawa, and N. Matsui, "New sustainable operation method for a power grid without an energy storage system: A case study of a hospital in Japan," International Journal of Renewable Energy Research (IJRER), vol. 12, no. 3, pp. 1289–1300, 2022.

[7] R. Jin, C. Lu, and J. Song, "Manage distributed energy storage charging and discharging strategy: Models and algorithms," IEEE Transactions on Engineering Management, vol. 69, no. 3, pp. 755–764, 2020.

[8] N. Christiansen, M. Kaltschmitt, and F. Dzukowski, "Electrical energy consumption and utilization time analysis of hospital departments and large scale medical equipment," Energy and Buildings, vol. 131, pp. 172–183, 2016.

[9] F. Angizeh, A. Ghofrani, E. Zaidan, and M. A. Jafari, "Resilience-oriented behind-the-meter energy storage system evaluation for mission-critical facilities," IEEE Access, vol. 9, pp. 80854–80865, 2021.

[10] A. Dogan, D. Guven, M. O. Kayalica, and A. A. Bayar, "Scheduling model for a trigeneration system with energy storage unit: A hospital application," IEEE Transactions on Engineering Management, vol. 71, pp. 6146–6159, 2024.

[11] R. Colucci, I. Mahgoub, H. Yousefizadeh, and H. Al-Najada, "Survey of strategies to optimize battery operation to minimize the electricity cost in a microgrid with renewable energy sources and electric vehicles," IEEE Access, vol. 12, pp. 8246–8261, 2024.

[12] S. Koli, S. Patil, B. B. S., S. Naik, K. R. Patil, and S. M., "Study of energy cost optimization for integration of microgrid to electric vehicles," in Proc. 3rd International Conference for Innovation in Technology (INOCON), Bangalore, India, 2024, pp. 1–6.

[13] H. Masrur, M. Shafie-Khah, M. J. Hossain, and T. Senjyu, "Multi-energy microgrids incorporating EV integration: Optimal design and resilient operation," IEEE Transactions on Smart Grid, vol. 13, no. 5, pp. 3508–3518, 2022.

[14] A. Abuelrub, F. Hamed, J. Hedel, and H. M. K. Al-Masri, "Feasibility study for electric vehicle usage in a microgrid integrated with renewable energy," IEEE Transactions on Transportation Electrification, vol. 9, no. 3, pp. 4306–4315, 2023.

[15] M. Ahmadigorji, M. Mehrasa, A. Labonne, A. Hably, and S. Bacha, "A robust multiobjective optimization strategy for power management in a PV-integrated G2V/V2G system," IEEE Transactions on Industrial Informatics, vol. 21, no. 8, pp. 5822–5833, 2025.

[16] A. AbuElrub, F. Hamed, and O. Saadeh, "Microgrid integrated electric vehicle charging algorithm with photovoltaic generation," Journal of Energy Storage, vol. 32, 101858, 2020.

[17] I. A. Zenhom, M. F. Shaaban, and W. A. Omran, "Grid interactive charging of EVs in PV-powered parking lots considering uncertainties," IEEE Access, vol. 11, pp. 111292–111301, 2023.

[18] I. Jokinen and M. Lehtonen, "Flexibility of electric vehicle charging with demand response and vehicle-to-grid for power system benefit," IEEE Access, vol. 12, pp. 131419–131441, 2024.

[19] N. Das, A. Haque, H. Zaman, S. Morsalin, and S. Islam, "Domestic load management with coordinated photovoltaics, battery storage and electric vehicle operation," IEEE Access, vol. 11, pp. 12075–12087, 2023.

[20] X. Liu, "Research on flexibility evaluation method of distribution system based on renewable energy and electric vehicles," IEEE Access, vol. 8, pp. 109249–109265, 2020.

[21] S. Li, P. Zhao, C. Gu, J. Li, S. Cheng, and M. Xu, "Battery protective electric vehicle charging management in renewable energy system," IEEE Transactions on Industrial Informatics, vol. 19, no. 2, pp. 1312–1321, 2023.

[22] F. Dincer and E. Ozer, "Numerical and experimental analysis of photovoltaic-integrated energy storage system for electric vehicle fast charging," IEEE Access, vol. 13, pp. 129127–129142, 2025.

[23] A. Wego, "Field test on energy flows in residential buildings with PV systems, heat pump based heating and battery electric car operation," in Proc. 2023 International Interdisciplinary PhD Workshop (IIPhDW), Wismar, Germany, 2023, pp. 1–4.

[24] A. Shukla, H. Shukla, S. K. Yadav, J. Singh, and R. B. Singh, "Solar powered electric vehicle charging station with integrated battery storage system," Energy Storage, vol. 6, no. 8, e70077, 2024.

[25] B. Singh, A. Verma, A. Chandra, and K. Al-Haddad, "Implementation of solar PV-battery and diesel generator based electric vehicle charging station," IEEE Transactions on Industry Applications, vol. 56, no. 4, pp. 4007–4016, 2020.

[26] K. Kumaoka, H. Morikawa, N. Matsui, J. Choi, and Y. Mizuno, "Determination of PV capacity for charging: A case study on the electrification of clinic shuttle services in Japan," in Proc. 14th International Conference on Renewable Energy Research and Applications (ICRERA), Vienna, Austria, 2025, pp. 1965–1969.

[27] A. P. Dobos, PVWatts Version 5 Manual, National Renewable Energy Laboratory (NREL), Golden, CO, USA, Tech. Rep. NREL/TP-6A20-62641, 2014.

[28] J. A. Duffie and W. A. Beckman, Solar Engineering of Thermal Processes, 4th ed. New York, NY, USA: John Wiley & Sons, 2013.

[29] Ministry of the Environment, Japan, "Renewable Energy Potential System (REPOS)," Available: https://repos.env.go.jp/web/. Accessed: Mar. 2026.

[30] W. F. Mbasso, I. Dagal, M. K. Singla, M. S. Shaikh, A. Smerat, A. M. Al Fatais, A. S. Almufih, and R. E. Al Mamlookol, "Drift-aware global intelligent optimization and advanced control of photovoltaic MPPT under complex operating conditions: A Cameroon case study," Energy Engineering, 2026, doi:10.32604/ee.2026.072751.

[31] W. F. Mbasso, A. Harrison, P. Jangir, I. Dagal, M. Khishe, A. Smerat, S. Chebaane, and T. Saidani, "Reliability-conscious power flow optimization in hybrid renewable microgrids: A case study in Sub-Saharan Africa using Gauss–Seidel and metaheuristic techniques," International Journal of Electrical Power & Energy Systems, vol. 173, 111350, 2025.

[32] A. Harrison, W. F. Mbasso, I. Dagal, N. H. Alombah, P. Jangir, S. F. Al-Gahtani, and Z. M. S. Elbarbary, "Environmental sensor-less hybrid analytical–machine learning (ESHAML) framework for ultra-fast solar irradiance estimation in climate-sensitive real-time applications: Experimental validation," Measurement, vol. 257, 118635, 2026.